PHYSICAL REVIEW D **90,** 064026 (2014)

Rotating protoneutron stars: Spin evolution, maximum mass, and I-Love-Q relations

Grégoire Martinon,[1,2,*] Andrea Maselli,[1,3,†] Leonardo Gualtieri,[1,3,‡] and Valeria Ferrari[1,3,§]

[1]*Dipartimento di Fisica, Sapienza, Università di Roma, Piazzale Aldo Moro 2, 00185 Roma, Italy*
[2]*Département de Physique, École Normale Supérieure de Cachan, 61 Avenue du Président Wilson, 94235 Cachan, France*
[3]*Sezione INFN Roma1, Piazzale Aldo Moro 2, 00185 Roma, Italy*

(Received 3 July 2014; published 12 September 2014)

Shortly after its birth in a gravitational collapse, a protoneutron star enters in a phase of quasistationary evolution characterized by large gradients of the thermodynamical variables and intense neutrino emission. In a few tens of seconds, the gradients smooth out while the star contracts and cools down, until it becomes a neutron star. In this paper we study this phase of the protoneutron star life including rotation, and employing finite-temperature equations of state. We model the evolution of the rotation rate, and determine the relevant quantities characterizing the star. Our results show that an isolated neutron star cannot reach, at the end of the evolution, the maximum values of mass and rotation rate allowed by the zero-temperature equation of state. Moreover, a mature neutron star evolved in isolation cannot rotate too rapidly, even if it is born from a protoneutron star rotating at the mass-shedding limit. We also show that the I-Love-Q relations are violated in the first second of life, but they are satisfied as soon as the entropy gradients smooth out.

DOI: 10.1103/PhysRevD.90.064026 PACS numbers: 04.40.Dg, 97.60.Jd, 04.25.Nx

I. INTRODUCTION

Soon after its birth in a gravitational collapse, a protoneutron star (PNS) is a hot and rapidly evolving object. The initial evolution, which lasts tens to a few hundreds of milliseconds, is characterized by strong instabilities of different nature. Then the PNS life becomes less hectic, and the star slowly evolves over time scales of the order of days to several thousand years, to reach the state of a mature, cold neutron star (NS).

The parameters of a newborn PNS carry the imprint of the supernova explosion mechanism, which is still quite poorly understood. For instance, it is presently not clear how fast a PNS can initially rotate, information which is instrumental in order to model the subsequent evolution of young pulsars.

To study this problem, two main approaches have been followed in the literature. The first is based on modeling the stellar evolution of the massive progenitor (typically $M \sim 10$–$30 M_\odot$) [1], and on numerical simulations of the collapse and of the supernova explosion. These simulations are performed either in Newtonian theory [2] or in full general relativity [3–5], and extend up to ∼100–1000 ms after the bounce. These studies indicate that, at this stage, the minimum rotation period of a PNS should range from few to ∼10 milliseconds. However, after the bounce several processes and instabilities are likely to spin down the PNS (see, e.g., [3,6] and references therein). These will be briefly discussed below.

A second approach is based on astrophysical observations of young pulsars [7,8]. In these works, the initial spin rate is inferred from the spin rates of observed pulsars, assuming that the star spins down according to the standard magnetodipole rule, and that no other dissipative mechanisms are effective. In [8] the authors, extending the work of [7], found that the initial spin period of a set of 30 young pulsars has a roughly flat distribution, from ∼10 ms to some hundreds of ms, with most of the pulsars having periods $\gtrsim$100 ms. This approach is appropriate to trace back the rotation rate up to some "initial" time when the star became a neutron star and dynamical processes were no longer effective. Thus, the two approaches cover two nonoverlapping parts of the stellar evolution.

However, something very interesting happens in between: after the turbulent phase which characterizes the first few hundreds of milliseconds after the bounce, the star undergoes a more quiet, "quasistationary" phase, which can be described as a sequence of equilibrium configurations [9–12]. The main macroscopic phenomena which characterize this part of the stellar life are the contracting from an initial 30–40 km radius to a final radius of 10–15 km, the star cooling, and the smoothing of the intense temperature-entropy gradients in the interior. To set an approximate time scale, we can say that this phase starts ∼200–500 ms after bounce and lasts for about 1 min. Neutrino processes are obviously very important during this time [9].

As the star contracts and cools down, its rotation rate changes. Therefore, modeling this part of the PNS life is important for understanding how to match the results of

*gregoire.martinon@ens-cachan.fr
†andrea.maselli@roma1.infn.it
‡leonardo.gualtieri@roma1.infn.it
§valeria.ferrari@roma1.infn.it

the studies on stellar evolution and supernova explosion with the rotation rates of young pulsars observed today.

We shall indicate the three main phases of the stellar evolution as *phase 1*, involving collapse and postbounce up to a few hundred milliseconds; *phase 2*, when the evolution is quasistationary; and *phase 3* when, having reached approximately its final radius, the star quietly cools down, and its spin rate decreases due to magnetodipole emission and possibly secular instabilities.

In this paper we are interested in modeling phase 2. Before going into the details of the modeling we would like to briefly discuss whether the numerous phenomena and instabilities, which can be active during the stellar evolution, may affect phase 2.

(i) Dynamical instabilities (e.g., bar mode, magnetohydrodynamical) act on a time scale of the order of the rotation period (for a detailed discussion, see [6,13,14]). They can only set in when the rotation period is very close to the mass-shedding limit (∼1–10 ms); therefore, they are expected to be suppressed before phase 2 sets in.

(ii) Secular instabilities (e.g., r-mode, f-mode instabilities) act on time scales ranging from ∼1 s to several years; they become effective at temperatures $T \lesssim 10^{10}$ K, typically reached after the first minute of life of the PNS [13–15]. In phase 2, the star is too hot ($T \gtrsim 10^{11}$ K) for secular instabilities to be effective (at least, excluding the case of quark stars or stars having exotic matter in the core).

(iii) Neutrinos carry away a significant part of the total mass (up to ∼20%) [9] and of the PNS angular momentum (up to ∼40% [16]). Neutrino processes are most effective in phase 1, during which most of the mass and angular momentum losses occur, but they may not be negligible in phase 2. This point will be further discussed in the following.

(iv) Strong magnetic winds may significantly spin down a rapidly rotating PNS, for surface fields as high as $\sim 10^{15}$–10^{16} G [1,6].

(v) It has recently been suggested [17] that due to the standing accretion shock instability (SASI), accretion of matter surrounding the PNS during the first second after the bounce can significantly spin up the PNS. However, subsequent, more accurate numerical simulations found that this process is not effective [18].

The above-listed processes are not fully understood; however, based on current literature, we shall assume that they are not effective in phase 2, i.e., between $t \sim 0.2$–0.5 s and $t \sim 1$ min after bounce, with the only exception of mass and angular momentum losses through neutrino emission. We will not include in our study the effects of extremely strong magnetic fields.

In the literature, several fully nonlinear and approximate numerical codes have been developed to find the structure of mature neutron stars, at the end of thermodynamical evolution. However, very few simulations have been performed to simulate a hot, rapidly rotating PNS. Fully numerical simulations have been performed in [19,20], assuming an isentropic or isothermal profile for the hot core, and in [21], employing a set of profiles previously obtained in [9] for a nonrotating PNS. In a series of papers published in the late 1960s, J. B. Hartle developed a perturbative approach which allows us to expand Einstein's equations for the structure of a rotating star at different orders in the angular velocity. The equations were derived assuming a barotropic equation of state (EoS), appropriate for describing a cold, old neutron star. Since we are interested in hot, newly born protoneutron stars, in this paper we generalize this approach to that case, at third order in the rotation rate, and solve the equations numerically using some equations of state which have been proposed in the literature to describe hot protoneutron stars.

We will compute the mass, radius, moment of inertia, and quadrupole moment for stellar sequences having fixed baryonic mass and varying angular velocity up to mass shedding.

In addition, we shall determine the evolution of the PNS rotation rate, while it cools and contracts during phase 2, under the assumption that the angular momentum decreases due to neutrino emission; we shall employ the heuristic formula proposed in [16] to describe the angular momentum carried away by neutrinos.

In recent years some universal relations have been shown to exist, which link the moment of inertia, the tidal deformability and the spin-induced quadrupole moment of mature neutron stars [22–27]. They are named "I-Love-Q" relations, and have been tested for cold equations of state ($T \lesssim 10^9$ K). In the last section of this paper, we will assess the range of validity of the I-Love-Q relations when applied to newly born, hot protoneutron stars.

II. PERTURBATIVE APPROACH TO ROTATING STARS EXTENDED TO NONBAROTROPIC EQUATIONS OF STATE

According to the perturbative approach introduced by Hartle [28], the metric describing a rotating star can be found by perturbing the spherical nonrotating metric in powers of the angular velocity Ω, expanded in Legendre polynomials. The resulting metric up to third order terms in Ω is

$$\begin{aligned} ds^2 = & -e^{\nu(r)}[1 + 2h_0(r) + 2h_2(r)P_2(\mu)]dt^2 \\ & + e^{\lambda(r)}\left[1 + \frac{2m_0(r) + 2m_2(r)P_2(\mu)}{r - 2M(r)}\right]dr^2 \\ & + r^2[1 + 2k_2(r)P_2(\mu)] \\ & \times [d\theta^2 + \sin^2\theta\{d\phi - [\omega(r) + w_1(r) \\ & + w_3(r)P_3'(\mu)]dt\}^2], \end{aligned} \tag{1}$$

where $\mu = \cos\theta$ and $P_n(\mu)$ is the Legendre polynomial of order n, the prime denoting the derivative with respect to μ. The functions ν, M, and λ are those commonly used to describe the nonrotating stars in the Tolman-Oppenheimer-Volkoff (TOV) equations. The function ω is of order Ω and is responsible for the dragging of inertial frames; it also determines the lowest order contribution to the star angular momentum. The functions h_0, m_0 and h_2, m_2, k_2 are all of order Ω^2, the former giving rise to spherical expansion, the latter to quadrupolar deformation. Finally, the functions w_1, w_3 are of order Ω^3 and are involved in corrections to the angular momentum as well as to the frame-dragging and mass-shedding limit (see [29] for details).

The energy-momentum tensor of the matter composing the star is

$$T^{\mu\nu} = (\mathcal{E} + \mathcal{P})u^\mu u^\nu + \mathcal{P}g^{\mu\nu} \tag{2}$$

where calligraphic, capital letters denote thermodynamical quantities (energy density and pressure) in the rotating configuration; u^μ are the components of the 4-velocity of the fluid; and $g_{\mu\nu}$ is the metric.

Due to rotation, an element of fluid located at a given (r,θ) in the nonrotating star is displaced to

$$\bar{r} = r + \xi(r,\theta), \tag{3}$$

where

$$\xi(r,\theta) = \xi_0(r) + \xi_2(r)P_2(\mu) + O(\Omega^4) \tag{4}$$

is the Lagrangian displacement, and both ξ_0 and ξ_2 are of order Ω^2. As a consequence of this displacement, all thermodynamical variables experience a local change which is found, following Hartle [[28], Eq. (71)], by setting to zero the Lagrangian variation of the considered quantity. For instance, for the pressure,

$$\Delta P = \delta P + \frac{dP}{dr}\delta r = 0 \rightarrow \delta P(r,\theta) = -\frac{dP}{dr}\xi(r,\theta). \tag{5}$$

Consequently, we can write

$$\delta P(r,\theta) = [\epsilon(r) + P(r)][\delta p_0(r) + \delta p_2(r)P_2(\mu)], \tag{6}$$

where ϵ and P are energy density and pressure computed by the TOV equations, and

$$\delta p_{0,2} = -\xi_{0,2}\left[\frac{1}{\epsilon + P}\frac{dP}{dr}\right], \tag{7}$$

and similarly for the Eulerian change of the energy density. It should be noted that, if the equation of state is barotropic $\epsilon = \epsilon(P)$, this change can be written as

$$\begin{aligned}\delta\epsilon &= -\frac{d\epsilon}{dr}\xi(r,\theta) \\ &= \frac{d\epsilon}{dP}[\epsilon(r) + P(r)][\delta p_0(r) + \delta p_2(r)P_2(\mu)],\end{aligned} \tag{8}$$

where $\frac{d\epsilon}{dP} = (d\epsilon/dr)/(dP/dr)$. However, since we are interested in generalizing Hartle's equations to the nonbarotropic case, when $\epsilon = \epsilon(p,s,Y_i)$, where s is the entropy per baryon and Y_i is the number fraction of the ith specie, we do not introduce the total derivative $\frac{d\epsilon}{dP}$ in the expression of the mass-energy density perturbation $\delta\epsilon$, as in Eq. (8). We simply write

$$\delta\epsilon = \frac{d\epsilon}{dr}\Big/\frac{dP}{dr}(\epsilon(r) + P(r))[\delta p_0(r) + \delta p_2(r)P_2(\mu)]. \tag{9}$$

We remark that in the case of a nonbarotropic EoS, in order to compute the mass-energy density ϵ and the total radial derivative $\frac{d\epsilon}{dr}$ for an assigned value of pressure, the entropy and the number fraction profiles, $s(P)$, $Y_i(P)$, must be specified.

Solving Einstein's equations is equivalent to solving a set of differential equations for all the perturbation functions defined above. These equations are summarized in the appendix of [29]. In the nonbarotropic case, there are only two differences with respect of the original derivation of [28,30]. The first is that, as discussed above, $d\epsilon/dP$ should be meant as a shorthand for $\frac{d\epsilon}{dr}/\frac{dP}{dr}$. Secondly, in [28] equations

$$\frac{d}{dr}\left(\delta p_0 + h_0 - \frac{\chi^2 r^3}{3(r-2M)}\right) = 0 \tag{10}$$

$$\delta p_2 + h_2 - \frac{\chi^2 r^3}{3(r-2M)} = 0 \tag{11}$$

are obtained by exploiting a first integral of Einstein's equations,

$$\text{const} = \frac{\mathcal{E} + \mathcal{P}}{u^t}\exp\left(-\int\frac{d\mathcal{E}}{\mathcal{E} + \mathcal{P}}\right). \tag{12}$$

To our knowledge, no such first integral exists in the nonbarotropic case. However, Eqs. (10) and (11) are still valid since they can be shown to follow from the divergence equation $T^{\mu\nu}{}_{;\nu} = 0$.

III. TESTS OF HARTLE'S PROCEDURE VERSUS FULLY RELATIVISTIC SIMULATIONS

In order to establish to what extent Hartle's procedure gives an accurate description of a rotating star, we have used five barotropic equations of state appropriate to describe mature neutron stars, named A, AU, APR, O, and G240 (see the Appendix for details), whose mass-radius relations are shown in Fig. 1. The reason why we choose these equations of state is that they span a large range of stellar compactness. Tests of Hartle's procedure for cold NSs have been done in several papers in the past to establish the relevance of terms of order $n+1$ in the rotation rate with respect to those of order n [29], or to compare the results of the numerical integration of Hartle's

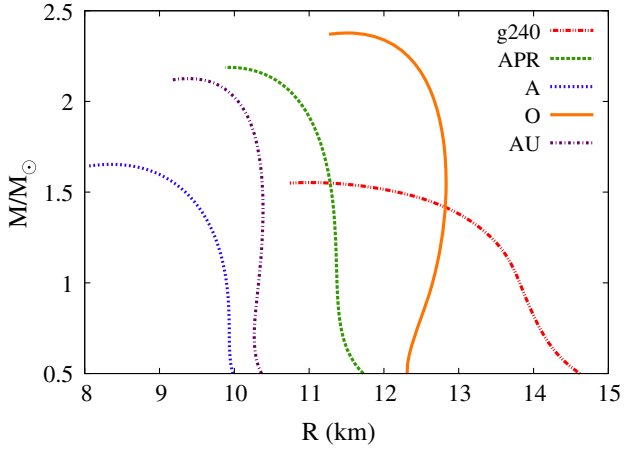

FIG. 1 (color online). Mass-radius diagram for the cold equations of state used to test Hartle's procedure versus RNS code results.

equations with those of fully relativistic, nonlinear codes [31–33]. Since we are interested in constructing sequences of newly born, rotating protoneutron stars, which are less dense than the cold NSs which form at the end of the evolution, we want to understand in particular how the accuracy of Hartle's procedure depends on the stellar compactness. Therefore, we have compared the results we obtain by integrating Hartle's equations for stars with fixed baryonic mass and different equations of state with those we find using the open source code RNS [34], which integrates the fully nonlinear equations of stellar structure. We would like to stress that this test is possible only for cold equations of state, since fully nonlinear codes for rapidly rotating, hot protoneutron stars are not publicly available. The quantities we compare are the mass, radius, and moment of inertia. We do not compare the quadrupole moment, because the computation of this quantity in the public version of RNS is affected by a systematic error [35]. Details on this comparison are given in the Appendix; here we summarize the results.

It is known that the mass-shedding rotation rate $\nu_{\rm ms}$ is systematically overestimated by the perturbative approach [29]. Therefore, we extend the comparison up to $\nu_{\rm ms}$ evaluated by the RNS code, and normalize the rotation rate to that value. We choose two values of the baryonic mass, $M_{\rm b} = 1.55M_\odot$ and $M_{\rm b} = 2.2M_\odot$. For $M_{\rm b} = 1.55M_\odot$ we consider the equations of state A, APR, and G240, whereas for $M_{\rm b} = 2.2M_\odot$ we consider the equations of state AU, APR, and O since the maximum mass of A and G240 is smaller than this value.

The results of the Hartle-versus-RNS comparison are given in Fig. 9 and in Table VII of the Appendix. These show that the two approaches produce values of the mass, equatorial radius (circumferential), and moment of inertia in good agreement (relative difference $\lesssim 5\%$ for rotation rates up to 0.8 of the mass-shedding limit), quite independently of the stellar compactness, and the EoS. This gives a strong indication for the reliability of Hartle's procedure when applied to hot and less dense stars, which is the case we are interested in.

In the next sections we shall apply Hartle's procedure to study the structure of newly born, rotating protoneutron stars. We shall extend our calculations up to the mass-shedding limit, keeping in mind the limitations on the accuracy discussed above.

IV. MODELS OF EVOLVING PNS

Numerical simulations of the early evolution of newly born protoneutron stars have shown that a few tenths of seconds after the bounce which follows a supernova explosion the evolution of the star can be considered as "quasistationary"; i.e., it can be described by a sequence of equilibrium configurations [9–12]. The main feature of this quasistationary phase is that, starting from an initial configuration characterized by a low-entropy core and a high-entropy envelope, due to neutrino processes the entropy gradient gradually smooths out, while the star progressively cools down, and eventually the overall entropy decreases.

To study how the structure of an evolving PNS depends on the rotation rate, we use two sets of nonbarotropic, hot stellar models, based on two different equations of state of baryonic matter. The first is a sequence of mass-energy, pressure, lepton fraction, and entropy profiles ("profiles" in short), indicated as GM3NQ to hereafter, based on an equation of state obtained within a finite-temperature, field-theoretical model solved at the mean field level [9–11]. These profiles were found by solving the relativistic equations of neutrino transport and nucleon-meson coupling, assuming a spherical spacetime background, and a NS baryonic mass $M_{\rm b} = 1.6M_\odot$, during the first minute of the stellar life. Thus, this is a true evolutionary sequence, and it refers to a unique baryonic mass. These models have been used to compute how the oscillation frequencies change as the star cools and contracts in [36] (Model A), [37], and in [38] to study how thermal diffusion affects the oscillation frequencies.

The second set of nonbarotropic, hot profiles we shall use, tagged as BS, are based on a microscopic EoS obtained within the Brueckner-Hartree-Fock nuclear many-body approach extended to the finite-temperature regime within the Bloch–De Dominicis formalism (see [39–42] and references therein for explicit details). These models can be used to "mimic" a PNS evolution, since each profile is characterized by an entropy gradient which reproduces the main features of the quasistationary evolution described above. Thus, even though they are not obtained as a result of a dynamical simulation, they can be considered as snapshots of different stages of the evolution. The BS profiles are specified by three parameters: the entropy per baryon in the core s_c, the entropy per baryon in the envelope s_e, and the leptonic fraction Y_e, which is assumed to be constant throughout the star. In the following, we will identify the

BS profiles with a particular choice of these three parameters with the label $\mathtt{Ss}_c\mathtt{Ss}_e$-$\mathtt{Y}_e$, as in [42]. We will use an additional profile at zero temperature, which will be tagged as T0.

It should be stressed that the BS profiles can be used to generate rotating stellar models using Hartle's procedure because for each value of the rotation rate we can change the value of the central energy density and find stellar configurations with assigned baryonic mass. This is not possible with the profiles GM3NQ, since they correspond to a fixed value of the baryonic mass and of the central energy density.

The BS profiles will be used in the next two sections to study how the structure of a protoneutron star changes as a function of the rotation rate. The evolutionary sequence GM3NQ will be used in Sec. VI to test the I-Love-Q relations.

V. HOT AND YOUNG NEUTRON STARS

In order to study the behavior of the relevant parameters of evolving protoneutron stars as a function of the rotation rate, it is useful to know their values for the nonrotating configurations having the same baryonic mass. In Table I we tabulate the gravitational mass, the radius, and the moment of inertia for a star with baryonic mass $M_{\rm b} = 1.6M_\odot$ belonging to the profiles GM3NQ and BS. As explained in Sec. IV, GM3NQ describes a true evolutionary sequence of a protoneutron star, and in the first column we give the time after collapse at which each quasistationary configuration has been computed (see [9] and [36] for details).

The sequence BS mimics the evolution of a star with entropy gradients similar to those of the GM3NQ sequence. These profiles are labeled as S1S5-032, S2S4-032, S1S2-023, and T0, where the first two numbers in each label indicate the entropy per baryon, respectively, in the core and in the envelope, and the last number is the lepton fraction. Thus, for instance, S1S5-032 corresponds to the largest entropy gradient between core and envelope, and a lepton fraction $Y_l = 0.32$. T0 is the zero-temperature end point of the BS sequence. A comparison of the entropy profile, mass, and radius of these configurations with those of the GM3NQ sequence indicates that the S1S5-032 protoneutron star is similar to that of the GM3NQ sequence corresponding to $t = 0.5$ s.

In Fig. 2 we show the energy density and the entropy profiles inside the stars belonging to the two families.

As in Table I, in Table II we show the stellar parameters of stars belonging to the BS sequence with $M_{\rm b} = 1.8M_\odot$ and $M_{\rm b} = 2.0M_\odot$.

A. Mass-shedding limit

As we know, Hartle's procedure overestimates the mass-shedding frequency [29]. To compute this quantity we shall use a different approach, based on fully relativistic simulations. In [43], using the RNS code a fit has been proposed,

$$\nu_{\rm ms}({\rm Hz}) = 45862\sqrt{\frac{M_0/M_\odot}{(R_0/1\ {\rm km})^3}} - 189, \qquad (13)$$

which relates $\nu_{\rm ms}$ to the mass M_0 and the radius R_0 of the nonrotating star. According to [43], Eq. (13) estimates $\nu_{\rm ms}$, independently of the EoS, with errors not larger than ~2%. The fit (13) has been obtained by fixing the central density and finding the maximum rotation rate as a function of the gravitational mass and radius given by the TOV equations. Since we are interested in studying fixed baryonic mass sequences, to use this fit we proceed as follows (see Fig. 3). We choose a value of $M_{\rm b}$ and find the corresponding TOV-central density ϵ_0. Then we increase the rotation rate by a small amount reaching, say, Ω_1, and find the mass and radius corresponding to the same $M_{\rm b}$ using Hartle's procedure. The central density of this configuration, ϵ_1, is smaller than ϵ_0. The mass and radius M_0 and R_0 computed with TOV for that central density are then inserted into the fit (13) to find the corresponding mass-shedding limit. If this value is larger than Ω_1, we proceed further by increasing the rotation rate by another small step, keeping $M_{\rm b}$ fixed, and iterate the procedure. If it is smaller than Ω_1, we stop and say that this is the mass-shedding limit of our

TABLE I. We compare some relevant parameters of the nonrotating configurations belonging to two models of evolving protoneutron stars with the same baryonic mass: GM3NQ and BS. GM3NQ describes a true evolutionary sequence of a protoneutron star, whereas the sequence BS mimics the evolution of a star with an EoS different from GM3NQ, and similar entropy gradients. For both sequences we tabulate the gravitational mass, the radius, the moment of inertia (normalized to $I^* = 10^{45}$ g × cm^2), and mass-shedding frequency evaluated using the fit (13).

$M_{\rm b} = 1.6M_\odot$									
GM3NQ	$M/M_\odot$	R (km)	I/I^*	$\nu_{\rm ms}$ (Hz)	BS	$M/M_\odot$	R (km)	I/I^*	$\nu_{\rm ms}$ (Hz)
$t = 0.2$ s	1.58	34.35	5.33	97	...	...	...	...	...
$t = 0.5$ s	1.56	23.78	3.75	306	S1S5-032	1.50	24.35	1.84	256
$t = 2$ s	1.53	15.78	2.44	718	S2S4-032	1.51	19.51	1.83	420
$t = 5$ s	1.50	13.61	2.00	931	S1S2-023	1.49	14.02	1.45	790
$t = 20$ s	1.47	12.91	1.76	1010	T0	1.43	11.80	1.41	1060

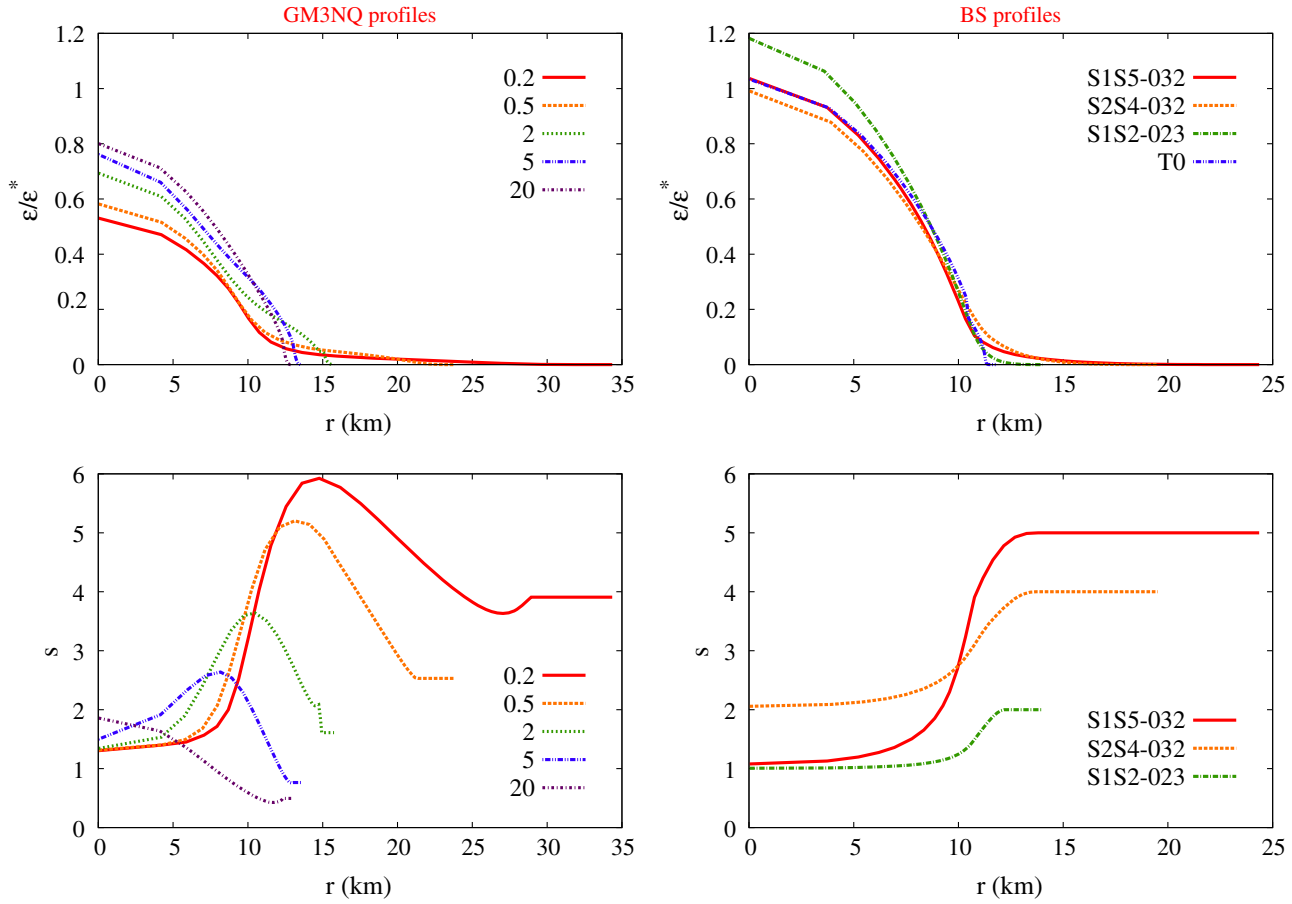

FIG. 2 (color online). The energy density and entropy per baryon versus radial distance are plotted for the two families of hot stars GM3NQ (left) and BS (right). The energy density (upper panel) is normalized to the value $\epsilon_* = 10^{15}$ g/cm^3. All plots refer to a nonrotating star with baryonic mass $M_b = 1.6M_\odot$.

rotating sequence with fixed baryonic mass. The accuracy of our iterative procedure (using Broyden's method) is of the order of 10^{-5}, which is smaller than the estimated accuracy of the fit.

The values of ν_{ms} evaluated with this procedure for the sequences GM3NQ and BS are given in the last columns

TABLE II. Parameters of the nonrotating stellar models BS, tabulated as in Table I, for baryonic mass $M_b = 1.8M_\odot$ and $M_b = 2.0M_\odot$.

EoS	$M/M_\odot$	R (km)	I/I^*	ν_{ms} (Hz)
		$M_b = 1.8M_\odot$		
S1S5-032	1.65	19.38	1.80	456
S2S4-032	1.67	16.84	1.87	596
S1S2-023	1.65	13.11	1.60	938
T0	1.59	11.62	1.59	1150
		$M_b = 2.0M_\odot$		
S1S5-032	1.79	16.41	1.85	658
S2S4-032	1.82	14.80	1.93	784
S1S2-023	1.80	12.20	1.72	1100
T0	1.74	11.37	1.76	1240

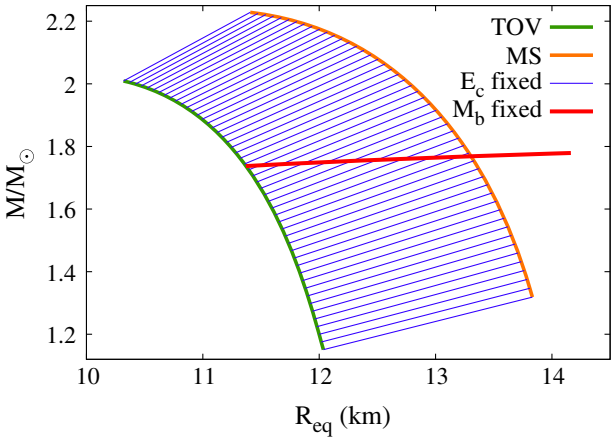

FIG. 3 (color online). This figure shows, for the profile T0, how we compute the mass-shedding limit using the fit (13). The thin, blue lines are sequences of stellar models with fixed central energy density ϵ_c and increasing rotation rate, from zero (where the blue lines intersect the TOV, zero rotation, green line) up to mass shedding given by Eq. (13), represented by the bold, yellow line. The thick, nearly horizontal red line is a sequence at fixed baryonic mass ($M_b = 2.0M_\odot$) and increasing rotation rate. The mass-shedding frequency is given by the intersection of this line with the bold, yellow line.

of Tables I and II. It is interesting to note that the mass-shedding frequencies of the initial configuration of each sequence are quite low and increase as the star cools down and contracts.

B. Rotating configurations

Starting from the nonrotating configurations belonging to the BS sequence, we can now construct models of rotating protoneutron stars. We choose a value of the baryonic mass and, keeping this value fixed, we use Hartle's procedure to find how the gravitational mass, the circumferential equatorial radius, the moment of inertia, and the quadrupole moment change as functions of the rotation rate. The results are shown in Fig. 4 for a star with $M_b = 1.6M_\odot$. For each profile of the BS sequence, the values of these quantities are plotted up to the corresponding mass-shedding limit ν_{ms} evaluated using the fit (13) and given in the last column of Table I. The behavior of M, R_{eq}, I, Q is similar to that of the cold stars shown in Fig. 9 (see the Appendix), and all quantities increase with rotation. However, there is a very interesting difference. The mass-shedding frequency of cold stars, for instance those considered in the Appendix, varies in the range $\sim$(800–1350) Hz for a star with $M_b = 1.55M_\odot$, i.e., by less than a factor 2 depending on the EoS. Conversely for the hot BS sequence it varies in a much broader range, being $\nu_{ms} = 256$ Hz for the "initial" configuration S1S5-032 and $\nu_{ms} = 1060$ Hz for the "final" configuration T0 (see Table I). This means that this protoneutron star cannot enter the quasistationary regime being very rapidly rotating, and that it can reach larger rotation rates only at subsequent times, as it contracts and cools down.

Rotation rates of newly born protoneutron stars can be larger if the baryonic mass is larger because ν_{ms} increases with M_b, as shown in Table II. In this case, the behavior of the relevant quantities is similar to that shown in Fig. 4 for $M_b = 1.6M_\odot$.

1. Mass-radius relation

Using the BS profiles we can construct the mass-radius diagram for rotating protoneutron stars. In Fig. 5 we show this diagram from the hottest, youngest configurations

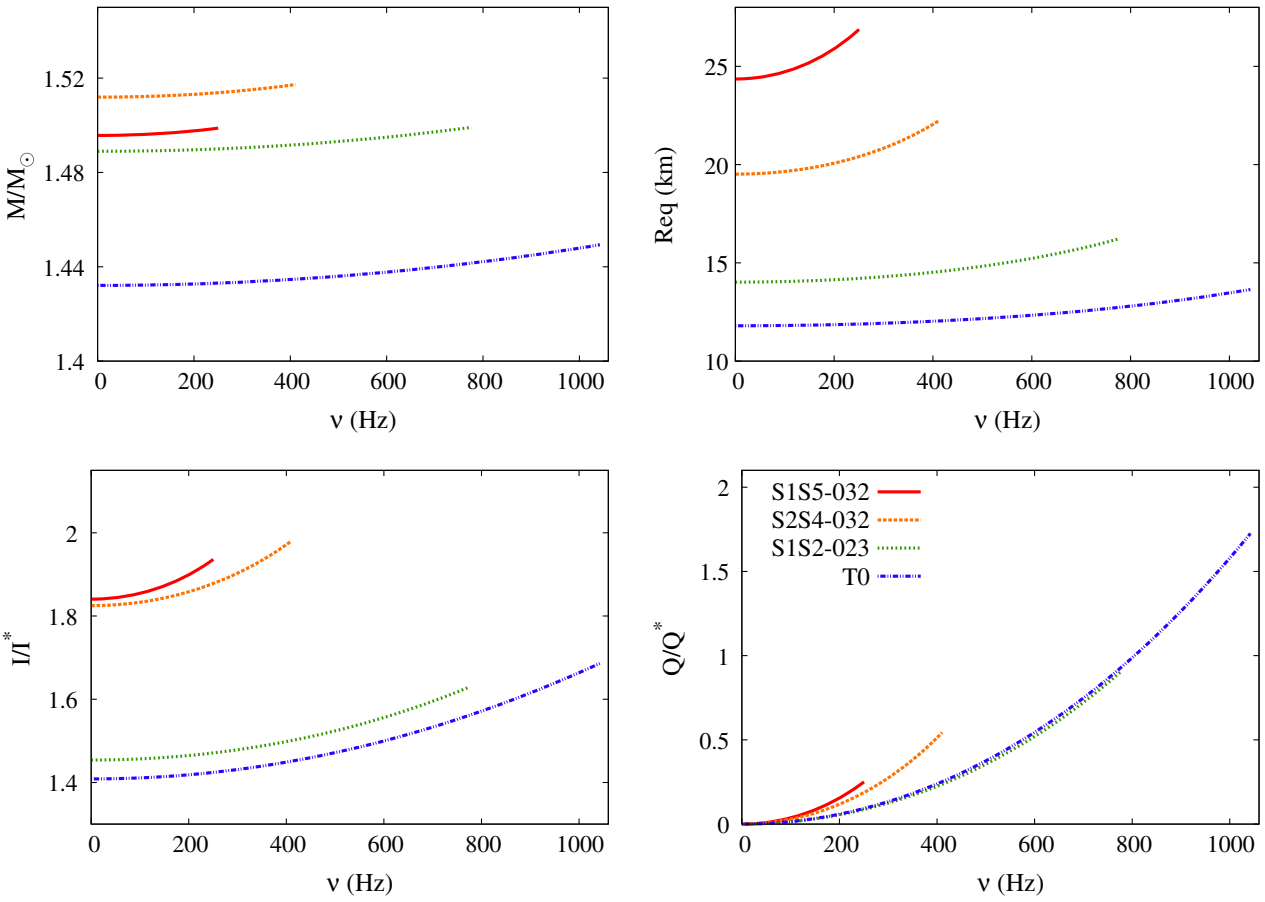

FIG. 4 (color online). The mass, equatorial radius, moment of inertia, and quadrupole moment of a star evolving according to the sequence of profiles BS shown in Fig. 2 are plotted as functions of the rotation rate. For each profile, the end point is the mass-shedding limit evaluated using the fit (13). All plots refer to a star with baryonic mass $M_b = 1.6M_\odot$. Moreover, $I^* = 10^{45}$ g $\times$ cm^2 and $Q^* = 10^{44}$ g $\times$ cm^2.

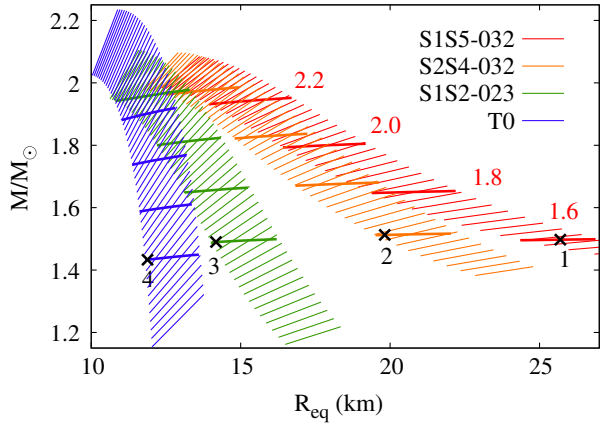

FIG. 5 (color online). Mass-radius diagram for four equations of state of the BS set. We have considered angular frequencies from 0 Hz up to the mass-shedding limit. Thick lines represent sequences at fixed baryonic masses $M_b = [1.6, 1.8, 2.0, 2.2]M_\odot$ (see text).

(high entropy gradient S1S5-032) to the coldest, oldest one (T0). For each profile, the thin, inclined lines indicate sequences at fixed central energy density. Each of these lines ends at the mass-shedding frequency evaluated with the fit (13). The bold, nearly horizontal lines are the sequences at fixed baryonic mass, with values $M_b = 1.6, 1.8, 2.0, 2.2\ M_\odot$.

As an example, let us consider the $M_b = 1.6M_\odot$ star with the S1S5-032 profile. This initial PNS configuration is a point on the lowest red bold line in Fig. 5, and its location on this line depends on the PNS angular velocity. We indicate the initial configuration with a 1 on the figure. As the star cools down, it is constrained to evolve, keeping the baryonic mass fixed; therefore, it will jump toward the left of the figure, reaching point 2 of the lowest bold line of the S2S4-032 profile (in this example we keep the angular momentum fixed as well). Then it will move to point 3 of the S1S2-023 profile and finally to point 4 of the cold, final T0 profile, always following the lowest bold lines. Thus, Fig. 5 can be understood as a "temporal" diagram. At the end of the evolution, the gravitational mass is smaller than that at the beginning. Since the maximum baryonic mass of the S1S5-032 profile is smaller than that of the final T0 profile, even if the initial mass of the star is close to the maximum mass allowed by the S1S5-032 profile, at the end of the quasistationary evolution it will have a gravitational mass smaller than the maximum mass allowed by the T0 profile.

We expect this feature to be independent of the particular evolutionary model we consider.

Thus, the maximum mass observed for an isolated neutron star is not constrained by the actual (cold) profile, but by the profile it had at the early stage of its life.

An interesting consequence of this result is the following. When the gravitational mass of a NS is known from astrophysical observations, the equations of state which predict a maximum mass larger than this value are considered compatible with the observation, while the others are ruled out [44]. However, our results show that this "compatibility test" is a necessary, but not sufficient condition: indeed, the final NS mass is the result of the evolution of a hot PNS, and the cold equations of state which should be "admitted" are those which result from an evolutionary sequence compatible with the observed mass.

2. Spin frequency change during the quasistationary evolution

We shall now consider a PNS with assigned baryonic mass and initial rotation rate ν_{in}. This star has the BS profile S1S5-032, which we consider as a model for a PNS at approximately 0.5 s from bounce. We want to compute how the spin frequency changes as the star evolves along the BS sequence, assuming either that angular momentum is conserved, or that a fraction of the angular momentum is lost due to neutrino emission. To model this second case, we use the empirical formula given in [16] (see also references therein):

$$\frac{J_{fin}}{J_{in}} = \left(\frac{M_{fin}}{M_{in}}\right)^{2.55}, \tag{14}$$

where J_{in}, M_{in} and J_{fin}, M_{fin} are the initial and final values of the angular momentum and of the star's gravitational mass. In our case, the final mass is that corresponding to the profile T0. The exponent of the mass ratio in Eq. (14) takes into account the shape and structure of the star as well as neutrino efficiency in removing angular momentum. The value 2.55 results from the most extreme case, when the angular momentum loss due to neutrinos is maximum.

We shall make the calculations for three values of the baryonic mass (kept fixed along the sequence) $M_b = 1.6, 1.8, 2.0\ M_\odot$, and for four values of the initial rotation rate, $\nu_{in} = (0.25, 0.5, 0.75, 1)\nu_{ms}$.

In Table III we show the results.

As an example, let us consider a PNS with $M_b = 1.6M_\odot$ which, a few hundreds of ms after bounce, has the profile S1S5-032. The mass-shedding frequency for this profile is $\nu_{ms} = 256$ Hz, and we assume that the star has initial rotation rate $\nu_{in} = 0.25\nu_{ms} = 64$ Hz. The angular momentum of this configuration is $J = 0.184$ km^2; the gravitational mass is $M_{in} = 1.50M_\odot$ (see Table I).

Using Hartle's procedure we evaluate the rotation rate that this star reaches at the end of the quasistationary evolution, when it has the profile T0, i.e., zero temperature, smaller radius, and moment of inertia, the same baryonic mass and smaller gravitational mass due to neutrino emission ($M_{fin} = 1.43M_\odot$). If we impose that the angular momentum is conserved, from Table III we see that the final rotation rate will be $\nu_{fin} = 83.8$ Hz, corresponding to 0.079 times the mass-shedding limit for the T0 profile,

TABLE III. Values of the spin frequency that a star, with a fixed baryonic mass and an initial rotation rate $\nu_{\rm in}$, reaches at the end of the quasistationary evolution, assuming that the angular momentum is conserved or that it changes due to neutrino emission. J is given in km^2, frequencies are in Hz. The initial values refer to a protoneutron star modeled with the profile S1S5-032, the final ones refer to the cold star with profile T0. Barred frequencies are normalized to the mass-shedding frequency of the initial and final profiles.

			J conserved			Neutrino losses		
$\bar{\nu}_{\rm in}$	$\nu_{\rm in}$	$J_{\rm in}$	$\bar{\nu}_{\rm fin}$	$\nu_{\rm fin}$	$J_{\rm fin}$	$\bar{\nu}_{\rm fin}$	$\nu_{\rm fin}$	$J_{\rm fin}$
$M_{\rm b} = 1.6M_\odot$ $(M_{\rm in} = 1.50M_\odot, M_{\rm fin} = 1.43M_\odot)$								
0.25	64.0	0.184	0.079	83.8	0.184	0.071	74.9	0.164
0.50	128	0.371	0.159	169	0.371	0.142	151	0.332
0.75	192	0.566	0.241	255	0.566	0.216	229	0.507
1.00	256	0.773	0.325	345	0.773	0.292	310	0.691
$M_{\rm b} = 1.8M_\odot$ $(M_{\rm in} = 1.65M_\odot, M_{\rm fin} = 1.59M_\odot)$								
0.25	114	0.321	0.112	129	0.321	0.102	118	0.293
0.50	228	0.651	0.226	260	0.651	0.206	237	0.593
0.75	342	0.997	0.341	392	0.997	0.312	359	0.908
1.00	456	1.37	0.461	530	1.37	0.423	486	1.25
$M_{\rm b} = 2.0M_\odot$ $(M_{\rm in} = 1.79M_\odot, M_{\rm fin} = 1.74M_\odot)$								
0.25	165	0.478	0.140	173	0.478	0.129	160	0.440
0.50	329	0.968	0.281	348	0.968	0.259	321	0.892
0.75	494	1.49	0.423	524	1.49	0.392	486	1.37
1.00	658	2.07	0.569	706	2.07	0.530	657	1.91

which is $\nu_{\rm ms} = 1060$ Hz. If, conversely, we assume that the angular momentum changes according to Eq. (14), the final spin frequency will be lower, $\nu_{\rm fin} = 74.9$ Hz, corresponding to ∼0.071 of the mass-shedding limit.

Thus, if the star is born with a rotation rate which is about one fourth of the mass-shedding limit, its rotation speed will remain slow even at the end, when the mass-shedding limit would, in principle, allow for larger rates.

If the star starts with a larger rotation rate, say, at the mass-shedding limit, at the end of the evolution its frequency will be larger, $\nu_{\rm fin} = 345$ Hz, or $\nu_{\rm fin} = 310$ Hz accounting for neutrino losses, but always smaller than the final mass-shedding limit. These considerations hold also for stars with larger baryonic mass.

Last but not least, the sequences we have considered show that the ratio $\nu/\nu_{\rm ms}$, even if large at the beginning of the evolution (large entropy gradient), constantly decreases as one goes along the cooling of the star. Thus, mature NSs evolved in isolation cannot rotate too rapidly, even if they are born from a PNS rotating at the mass-shedding limit.[1]

We have further explored the entire range of initial spin rate, from zero to the mass-shedding limit, computing the corresponding final spin frequency, for different values of the baryonic mass. In Fig. 6 we plot the relative difference $(\nu_{\rm fin} - \nu_{\rm in})/\nu_{\rm in}$, for the considered values of the baryonic mass, as a function of $\nu_{\rm in}$. We see that for the lightest star the change reaches ∼35% without including neutrino emission, and ∼25% with neutrino emission, whereas for the heaviest star the percent change does not exceed ∼5%. In this case it should be noted that the change may be negative for small values of $\nu_{\rm in}$, showing that stellar

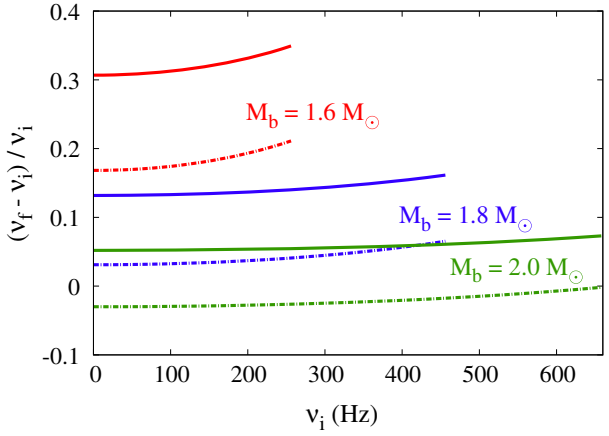

FIG. 6 (color online). We show the relative difference between the initial and final spin frequency, as a function of the initial spin rate, spanning the range from zero to the mass-shedding limit. The results are shown for three values of the baryonic mass; continuous lines refer to an evolution which assumes angular momentum conservation, and dashed lines to neutrino emission.

[1]We would like to remind the reader that from a naive point of view, a spherical Newtonian fluid ball has angular momentum $I\Omega \propto MR^2\Omega$ and mass-shedding limit $\propto M^{1/2}R^{-3/2}$. A factor 2 of decrease in radius would lead to an increase of a factor 4 in Ω and of a factor $\sqrt{8} \sim 3$ in the mass-shedding limit, thus allowing the final configuration to be close to the mass-shedding limit if the initial one was.

contraction due to the cooling, and neutrino emission could be competitive in some regime. This last result is EoS dependent, but still provides a proof of concept.

It should also be recalled that, as shown in Sec. III and in the Appendix, values of frequency too close to the mass-shedding limit are associated to larger errors on the various quantities, which for the moment of inertia can reach $\sim 11\%$; however, the errors rapidly decrease for lower rotation rates.

The early evolution of a PNS has also been studied in [45], using a mean field EoS [based on a chiral $SU(3)$ description of baryons] and assuming isentropic or isothermal profiles. They compute the maximum mass and the mass-shedding frequency for different values of entropy and temperature, assuming constant baryonic mass and constant angular momentum. This is different from what we do, since they do not compute the evolution of the gravitational mass and of the rotation rate.

There is another process which may subtract angular momentum to the PNS, if this is born with a certain degree of asymmetry: gravitational wave (GW) emission. If the PNS has a quadrupole ellipticity ϵ and rotates about an axis misaligned with the symmetry axis by an angle α, it emits GWs with luminosity $L_{\rm GW} \sim \frac{G}{c^5}\Omega^6\epsilon^2 I^2 \sin^2\alpha(16\cos^2\alpha + \sin^2\alpha) < \frac{G}{c^5}\Omega^6\epsilon^2 I^2$ [46]. However, the spin-down induced by GWs during the quasistationary evolution is negligible with respect to the spin-up due to contraction. A simple estimate shows that $\frac{\delta\Omega}{\Omega} \sim -\frac{L_{\rm GW}\delta t}{I\Omega^2} - \frac{\delta I}{2I}$; assuming for instance $\epsilon \sim 10^{-4}$ (see, e.g., [47]), $I \sim 10^{45}$ g $\times$ cm^2, $\Omega \sim 1$ kHz kHz, and considering that in a time scale $\delta t \sim 20$ s the moment of inertia is reduced by a factor ~ 2, the GW contribution to the spin-down is $\sim 10^6$ smaller than that due to contraction. During the first few hundreds of milliseconds after bounce, the GW signal is expected to be dominated by processes associated to neutrino emission, magnetorotational processes, SASI, dynamical instabilities, etc. [4,48,49]. However, we have just shown that when the evolution becomes quasistationary the signal could be dominated by the spin-up due to contraction. Thus in this phase, which would last for about a minute, the signal would be "chirplike," and this feature may be searched for in the postprocessing of the data associated to a GW signal from a supernova with appropriate data analysis techniques.

Finally, we would like to mention that in our study we did not include the effect of differential rotation, which may be present in the very early stages of the PNS evolution. This effect will be studied in a separate paper.

VI. I-LOVE-Q RELATIONS FOR HOT AND YOUNG NEUTRONS STARS

As discussed in the Introduction, it has recently been found that the moment of inertia (I), the tidal deformability (λ), and the spin-induced quadrupole moment (Q) of isolated and binary neutron stars are related by universal relations which are independent of the star's internal composition [22–26] (further universal relations have been studied in [50–53]).

Until now, such I-Love-Q relations have been tested only for cold equations of state. In [22,23] two finite-temperature equations of state are also employed, LS220 and Shen. However, they are treated as barotropic, assuming a uniform temperature of $T \simeq 10^9$ K and no neutrinos: they describe the star more than 1 min after the bounce.

In this section, we will assess the range of validity of the universal relations for newly born stars, in which an entropy gradient between the core and the envelope is still present.

Before discussing our results, we shall briefly retrace the main steps needed to find the relativistic Love numbers. Let us consider a static, spherically symmetric star placed in a static, external, quadrupolar tidal field C_{ij}. This field induces a perturbation on the star structure. To linear order, the tidal deformability λ connects the star-induced quadrupole moment Q_{ij} with the external tidal field,

$$Q_{ij} = -\lambda C_{ij}, \tag{15}$$

and it is related to the dimensionless Love number

$$k_2 = \frac{3}{2}\frac{\lambda}{R^5}. \tag{16}$$

Both the star's quadrupole moment and the tidal field are defined in terms of an asymptotic expansion of the metric at large distance from the star, which can be computed by considering linear static perturbations expanded in spherical harmonics. The full metric is given by

$$g_{\alpha\beta} = g^{(0)}_{\alpha\beta} + h_{\alpha\beta}, \tag{17}$$

where $g^{(0)}_{\alpha\beta}$ describes the geometry of the static star, and $h_{\alpha\beta}$ is the metric perturbation:

$$h_{\alpha\beta} = \mathrm{diag}[-e^{\nu(r)}H_0(r), e^{\lambda(r)}H_2(r), r^2K(r), r^2\sin\theta K(r)]Y_{2m}(\theta,\phi). \tag{18}$$

$\nu(r)$ and $\lambda(r)$ are the zero order components of the metric tensor. Einstein's equations written for the metric Eq. (17) give a constraint, $H_0 = -H_2 = H$, and a relation between $H(r)$ and $K(r)$. Furthermore, they lead to a second order differential equation for $H(r)$. We refer the reader to [54] for details. The Love number is finally obtained as

$$\begin{aligned} k_2 = {} & \frac{8\mathcal{C}^5}{5}(1-2\mathcal{C})^2[2+2\mathcal{C}(y-1)-y]\{2\mathcal{C}[6-3y \\ & +3\mathcal{C}(5y-8)]+4\mathcal{C}^3[13-11y+\mathcal{C}(3y-2) \\ & +2\mathcal{C}^2(1+y)]+3(1-2\mathcal{C})^2[2-y \\ & +2\mathcal{C}(y-1)\ln(1-2\mathcal{C})]\}^{-1}, \end{aligned} \tag{19}$$

where $\mathcal{C} = M/R$ is the neutron star compactness and $y = H'(R)R/H(R)$.

TABLE IV. Best-fit coefficients of Eq. (20) for the I-Love-Q relations [22].

y	x	a	b	c	d	e
$\bar{I}$	$\bar{\lambda}$	1.47	0.0817	0.0149	0.000287	-3.64×10^{-5}
$\bar{I}$	$\bar{Q}$	1.35	0.697	−0.143	0.0994	-1.24×10^{-2}
$\bar{Q}$	$\bar{\lambda}$	0.194	0.0936	0.0474	−0.00421	1.23×10^{-4}

We will now compare the numerical data obtained by computing the I-λ-Q trio for NSs described by the profiles GM3NQ (see Sec. IV), with the relations originally found in [22,23]. We remind the reader that the GM3NQ profiles describe the evolution of a hot protoneutron star with baryonic mass $M_{\rm b} = 1.6M_{\odot}$ during the first minute of life after the gravitational collapse.

The fits have the following functional form:

$$\ln y = a + b\ln x + c(\ln x)^2 + d(\ln x)^3 + e(\ln x)^4 \quad (20)$$

where (a, b, c, d, e) are fitting coefficients listed in Table IV. Equation (20) is defined in terms of the normalized variables $(\bar{I}, \bar{Q}, \bar{\lambda})$, where $\bar{I} = I/M^3$, $\bar{\lambda} = \lambda/M^5$, and $\bar{Q} = Q(M/J^2)$, M being the neutron star's gravitational mass and J its angular momentum. We have computed $\bar{I}$, $\bar{\lambda}$, and $\bar{Q}$ for the GM3NQ protoneutron star at different stages of evolution, i.e., at $t = (0.2, 0.3, 0.5, 1, 2, 5, 20)$ s after birth. The corresponding values are shown in Table V.

In order to determine the accuracy within which the I-Love-Q relations would describe the features of a newly born neutron star, we have computed the relative errors $\Delta I/\bar{I}_{\rm fit} = |\bar{I} - \bar{I}_{\rm fit}|/\bar{I}_{\rm fit}$ and $\Delta Q/\bar{Q}_{\rm fit} = |\bar{Q} - \bar{Q}_{\rm fit}|/\bar{Q}_{\rm fit}$, between our numerical data, and those obtained by using the fit (20).

The results are summarized in the three panels of Fig. 7, which clearly show that the I-Love-Q relations lose their validity in the very early stages after the star's birth, with discrepancies between the analytic fit and the numerical values which can be as high as ∼30% at $t = 0.2$ s, for the $\bar{I}$-$\bar{Q}$ pair (middle panel in Fig. 7).

TABLE V. Parameters of the NS models with baryonic mass $M_{\rm b} = 1.6M_{\odot}$ built with the GM3NQ EoS. In the first column we show the time after the star's birth. In the remaining columns we list the gravitational mass M, the radius at spherical equilibrium, the quadrupole moment $\bar{Q}$, the moment of inertia $\bar{I}$, and the tidal deformability $\bar{\lambda}$.

t (s)	$M(M_{\odot})$	R (km)	$\bar{Q}$	$\bar{I}$	$\bar{\lambda}$
0.2	1.58	34.39	18.86	31.32	12999.60
0.3	1.57	28.98	15.23	26.83	7374.64
0.5	1.56	23.79	12.04	22.59	3630.51
1	1.55	19.38	9.40	18.70	1914.93
2	1.53	15.76	7.39	15.58	945.85
5	1.50	13.61	6.20	13.56	564.98
20	1.47	12.91	5.80	12.83	458.91

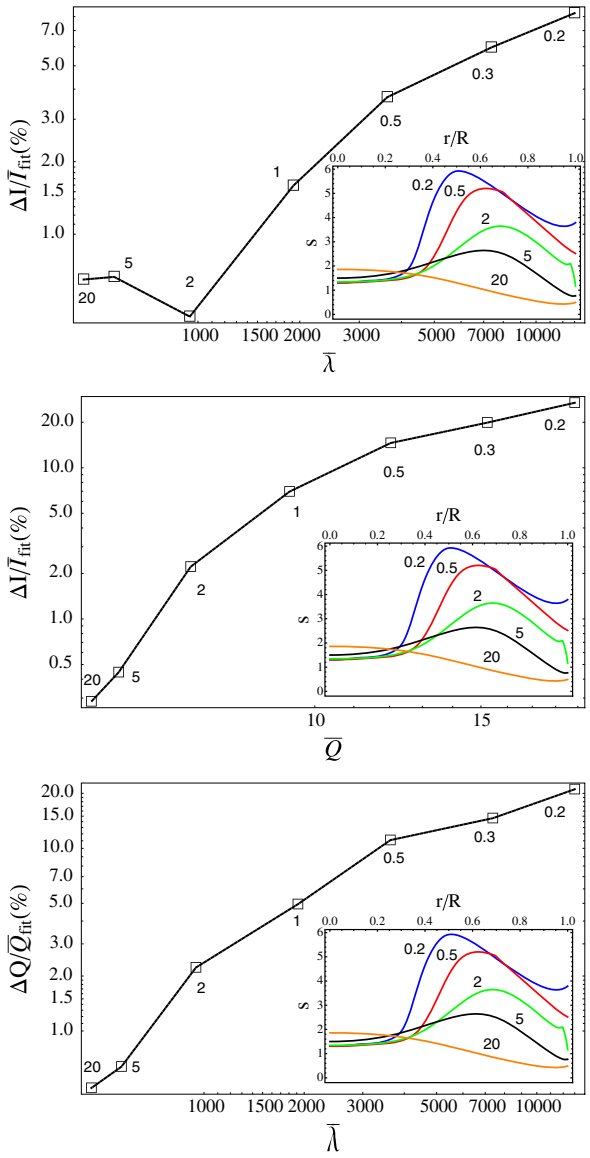

FIG. 7 (color online). We show the relative differences $|\bar{I} - \bar{I}_{\rm fit}|/\bar{I}_{\rm fit}$ and $|\bar{Q} - \bar{Q}_{\rm fit}|/\bar{Q}_{\rm fit}$ obtained by testing the universal relations (20) against the numerical data computed using the GM3NQ equations of state, at different times (in seconds) after the birth of the protoneutron star. In the inset we also show, for some of the considered configurations, the entropy per baryon as function of the star's radius.

However, the relative errors rapidly decrease as time increases: after 1 s, the relative difference between our moment of inertia and the fit $\bar{I}$-$\bar{\lambda}$ is 1.6%, that with respect to the fit $\bar{I}$-$\bar{Q}$ is 6.7%, and the relative difference between our quadrupole moment with respect to the fit $\bar{Q}$-$\bar{\lambda}$ is 4.8%. After 2 s, these errors reduce to $< 1\%$, 2.2%, and 2.0%, respectively. It it interesting to analyze these results in terms of the entropy gradient inside the star at different times. In each plot of Fig. 5 we have included the plot of the

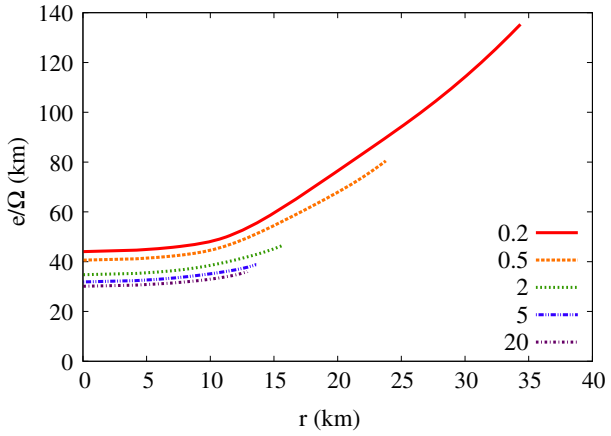

FIG. 8 (color online). The ellipticity of the isodensity contours, normalized to the rotation rate, is plotted as a function of the radial distance at different times of the PNS evolution. This plot refers to the GM3NQ quasistationary sequence with $M_b = 1.6M_\odot$.

entropy per baryon as a function of the distance from the center of the star (normalized to the radius R), for some of the considered configurations. This shows that the largest relative errors correspond to the higher entropy gradients inside the star (blue and red curves), which develop after its birth and smooth down during the following evolution. Thus, the time interval during which the I-Love-Q relations are accurate depends on how fast the star reaches the quiet state of a neutron star.

It has recently been suggested [55] that the I-Love-Q relations become less accurate when the ellipticity of the isodensity contours has a large gradient inside the star. In Fig. 8 we show the behavior of the ellipticity e of the isodensity contours [see Eq. (25c) of [56]], normalized to the star's rotation rate, for the GM3NQ quasistationary sequence with $M_b = 1.6M_\odot$ considered in this section. We see that in the first second after bounce, when the I-Love-Q relations are violated, the ellipticity exhibits significant variations throughout the star ($\gtrsim$200%). At later times, when the entropy profiles smooth out and the I-Love-Q relations are satisfied, the ellipticity profiles are nearly constant. This supports the suggestion of [55] that the validity of the I-Love-Q relations is associated with the self-similar isodensity condition.

VII. CONCLUDING REMARKS

In this paper we have studied how rotation affects the quasistationary evolution of newly born protoneutron stars. We have used Hartle's perturbative approach at third order in the angular velocity, which we have extended to describe warm stars, with nonbarotropic equations of state. Hartle's equations have been integrated to show how the rotation rate of a PNS with fixed baryonic mass changes during the evolution, taking into account neutrino losses in a heuristic way.

To model the PNS we have used an EoS obtained within the nuclear many-body theory extended to finite temperature [39–42], and a sequence of entropy and energy density profiles which mimics the stellar interior of a PNS. This is supposed to evolve from a few tenths of a second after bounce [temperature ~30–40 MeV (~5×10^{11} K), radius ~30 km, strong entropy gradients], to the following minute(s) during which gradients are smoothed out, temperature decreases to a few MeV, and radius decreases to 10–15 km.

The EoS and profiles we have used are constructed, having as a reference the quasistationary evolution profiles obtained in [9], by solving Boltzman's equation and using an EoS obtained within a finite-temperature, field-theoretical model solved at the mean field level. To our knowledge, the stellar models given in [9] are the only example of the quasistationary evolution of a nonrotating PNS available in the literature (we also mention the numerical simulations of [57,58], which employ equations of state very similar to those used in [9], and find similar results). Unfortunately we could not use these models to study how they change with rotation, because they are given for fixed values of the central energy density, whereas to generate a rotating star with fixed baryonic mass, we need to change it. However, we believe that the results we obtain in this paper with the BS sequence give interesting indications on the quasistationary evolution of a rotating, hot PNS, provided no instability is present (see discussion in Sec. I), and show a methodology which could be used with other stellar models of evolving PNS, when available.

Our main results are the following:

(i) As a PNS cools down, the maximum mass allowed by the EoS and by the chosen entropy profiles increases, and the maximum rotation rate (mass-shedding limit) increases as well.

(ii) A cold neutron star cannot have the maximum mass allowed by the final zero temperature EoS, unless the evolutionary path of the hot PNS from which it has evolved is allowed to do so. It is commonly believed that an equation of state is able to describe a NS interior if the maximum mass it predicts is larger than the maximum mass observed in neutron stars. However, our results show that this should be considered as a necessary, but not sufficient condition. This means that a full understanding of NS structure cannot overlook the history of these objects.

(iii) An isolated neutron star, even when born rotating near the mass-shedding limit, cannot have a rotation rate close to the mass-shedding limit associated to the cold EoS which characterizes its interior (see Table III and Fig. 6).

(iv) If an isolated NS is found to be rapidly rotating, Table III indicates that its mass must be high.

(v) I-Love-Q relations are no longer valid for very hot neutron stars, but become valid all the same a few

seconds after the bounce. Indeed our results show that such relations strongly depend on the entropy profile developing inside the star, and that their universality character is recovered as soon as entropy gradients smooth out during the evolution.

This work should (and will) be extended in many ways to include more realistic physics (e.g., differential rotation, magnetic fields, dynamical neutrino leakage, etc.) and a more accurate description of the PNS evolution.

ACKNOWLEDGMENTS

We would like to thank Fiorella Burgio, Hans-Joseph Schultze, and José Pons for kindly allowing us to use the profiles describing the early evolution of a protoneutron star. We also thank Morgane Fortin and Georgios Pappas for useful comments and discussions. This work was partially supported by "NewCompStar" (COST Action MP1304).

APPENDIX

In this appendix we compare some relevant stellar quantities computed by integrating Hartle's equations at third order in Ω (Hartle's results to hereafter), with those computed by using the fully relativistic code RNS (RNS results to hereafter). In particular, we compute the mass, radius and moment of inertia.

A few words about the equations of state we use for this comparison:

(i) A: EoS obtained in [59] using many-body theory, and named EoS A in [60]. Matter is composed of neutrons only. Interactions include a Reid soft core adapted to nuclear matter. The many-body Schrödinger equation is solved with a variational approach, applied to the correlation function.

(ii) AU: EoS named AV14 + UVII in [61], matched to Negele and Vautherin [62] at low densities. Based on variational methods with correlation operators on a Hamiltonian featuring the Argonne v_{14} two-nucleon potential with the Urbana VII three-nucleon potential.

(iii) APR: EoS obtained in [63] using many-body theory. Matter is composed of protons, neutrons, electrons, and muons. Interactions are described by the Argonne v_{18} two-nucleon potential and the Urbana VII three-nucleon potential, including relativistic corrections arising from the boost to a frame in

TABLE VI. Parameters of the nonrotating stellar configurations which we use to compare the results of the perturbative approach to those of fully relativistic calculations. $\bar{\rho} = \sqrt{M/R^3}$.

	G240	APR	A	O	APR	AU
M_b		$1.55M_\odot$			$2.2M_\odot$	
$M/M_\odot$	1.41	1.39	1.36	1.91	1.87	1.85
R (km)	12.84	11.33	9.61	12.74	11.05	10.25
$\bar{\rho}$ (km^{-1})	0.031	0.038	0.048	0.037	0.045	0.050
M/R	0.16	0.18	0.21	0.22	0.25	0.27

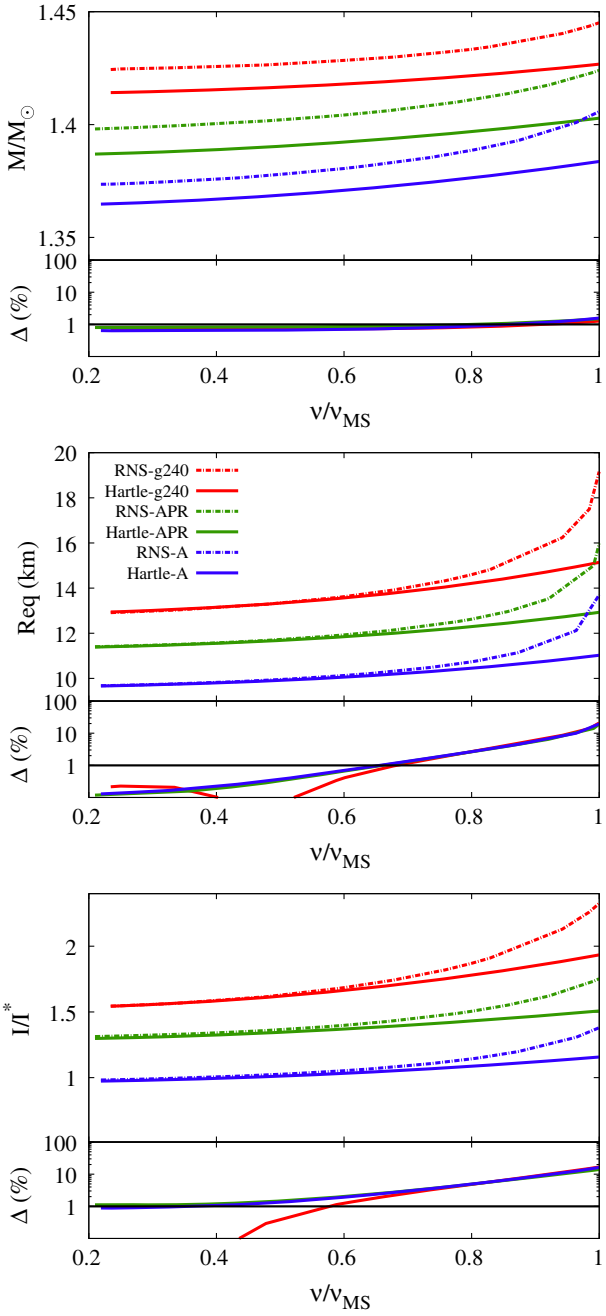

FIG. 9 (color online). We plot the mass, equatorial radius, and moment of inertia (normalized to $I^* = 10^{45}$ g × cm^2), as a function of the rotation rate normalized to the mass-shedding frequency. Solid and dashed lines indicate data computed by integrating Hartle's equations and using the RNS code, respectively. All data refer to a baryonic mass $M_b = 1.55M_\odot$ and the equations of state A, APR, and G240. In the lower part of each panel, we show the relative difference between the data computed using the two approaches.

TABLE VII. In this table we compare the values of the average density $\propto \sqrt{M/R_{\rm eq}^3}$, compactness $M/R_{\rm eq}$, equatorial radius $R_{\rm eq}$, and moment of inertia I (normalized to $I^* = 10^{45}$ g $\times$ cm^2), found using Hartle's procedure and the RNS code. Data refer to two values of the baryonic mass, $M_{\rm b} = 1.55, 2.2 M_\odot$, and different equations of state appropriate to describe cold stars with that mass. For each quantity we also show the relative difference between RNS and Hartle's results. The comparison is done for two values of the rotation rate, i.e., $\nu/\nu_{\rm ms} = 0.6$ and $\nu/\nu_{\rm ms} = 0.8$.

	$M_{\rm b} = 1.55 M_\odot$						$M_{\rm b} = 2.2 M_\odot$					
	G240	APR	A	G240	APR	A	O	APR	AU	O	APR	AU
$\nu/\nu_{\rm ms}$		0.6			0.8			0.6			0.8	
ν (Hz)	500	653	810	670	871	1080	650	793	900	860	1057	1200
$\nu_{\rm ms}$ (Hz)	833	1089	1350	833	1089	1350	1069	1321	1495	1069	1321	1495
$\sqrt{M/R_{\rm eq}^3}$ (km^{-1})	0.029	0.035	0.045	0.027	0.032	0.042	0.035	0.042	0.048	0.033	0.039	0.045
$M/R_{\rm eq}$	0.15	0.17	0.20	0.15	0.16	0.20	0.21	0.24	0.26	0.21	0.23	0.25
$M^{\rm Har}/M_\odot$	1.42	1.39	1.37	1.42	1.40	1.38	1.92	1.89	1.86	1.93	1.90	1.87
$M^{\rm rns}/M_\odot$	1.43	1.40	1.38	1.43	1.41	1.39	1.94	1.90	1.87	1.95	1.92	1.89
Δ (%)	1	1	1	1	1	1	1	1	1	1	1	1
$R_{\rm eq}^{\rm Har}$ (km)	13.57	11.85	10.06	14.20	12.29	10.45	13.32	11.53	10.67	13.81	11.96	11.05
$R_{\rm eq}^{\rm rns}$ (km)	13.63	11.93	10.13	14.60	12.63	10.74	13.42	11.60	10.74	14.17	12.25	11.32
Δ (%)	< 1	1	1	3	3	3	1	1	1	3	2	2
$I^{\rm Har}/I_*$	1.66	1.37	1.03	1.78	1.43	1.09	2.70	2.08	1.85	2.83	2.18	1.93
$I^{\rm rns}/I_*$	1.69	1.40	1.05	1.87	1.51	1.14	2.76	2.12	1.88	2.99	2.28	2.03
Δ (%)	2	2	2	5	5	4	2	2	2	5	4	5

which the total momentum of the interacting pair is nonvanishing.

(iv) O: EoS obtained in [64] and named as O in [60]. Matter is composed of neutrons, protons, and hyperons. Interactions are nonperturbative; it is a phenomenological approximation to relativistic meson exchange. The many-body theory is based on relativistic finite density Green's functions.

(v) G240: Obtained in [65,66]. Matter composition includes leptons and the complete octet of baryons (nucleons, $\Sigma^{0,\pm}$, Λ^0, and $\Xi^\pm$). Hadron dynamics is described in terms of exchange of one scalar and two vector mesons. The EoS is obtained within the mean field approximation.

The stellar parameters of the nonrotating configurations are given in Table VI. The results of the Hartle-versus-RNS comparison are given in Fig. 9 and in Table VII. In the three panels of Fig. 9, we compare mass, equatorial radius, and moment of inertia computed by integrating Hartle's equations (solid lines) and using the RNS code (dashed lines). All quantities are plotted versus the rotation rate normalized to the mass-shedding limit rate (computed with RNS), and are given for a star with baryonic mass $M_{\rm b} = 1.55 M_\odot$ and equations of state, A, APR, and G240. In the lower part of each panel we also show the percent difference between Hartle's and RNS results.

In Table VII we tabulate M, $R_{\rm eq}$, I for two values of the baryonic mass $M_{\rm b} = (1.55, 2.2) M_\odot$ and two values of the rotation rate, $\nu = (0.6, 0.8)\nu_{\rm ms}$. The superscripts "Har" and "rns" indicate that the values have been obtained using the Hartle procedure and the RNS code, respectively. For each quantity we also provide the relative difference between the two approaches. In addition, we show the average density, $\sqrt{M/R_{\rm eq}^3}$, and the compactness $M/R_{\rm eq}$ of the star.

Figure 9 and Table VII show that the relative difference between Hartle's and RNS results is

(i) less than 1% for the gravitational mass for rotation rates $\lesssim 0.9\nu_{\rm ms}$, where $\nu_{\rm ms}$ is the mass-shedding rotation rate evaluated with RNS, for all considered equations of state;

(ii) less than 3% for the equatorial radius up to $\lesssim 0.8\nu_{\rm ms}$;

(iii) less than 5% for the moment of inertia up to $\lesssim 0.8\nu_{\rm ms}$;

We have checked that our results are independent of the resolution. Doubling the number of grid points, all computed values change by less than 0.5%.

A similar comparison between perturbative and fully nonlinear codes has been done in [33], by using Hartle's procedure at second order in the rotation rate and the RNS code. They were focused on the evaluation of the innermost stable circular orbit and of the quadrupole moment which, however, was affected by the RNS error mentioned in Sec. III.

We also mention that in [53] Hartle's perturbative approach has been extended up to fourth order in the rotation rate, increasing the agreement with fully relativistic computations. However, a comparison with their results is not straightforward, because they are focused on the determination of universal relations for higher order multipole moments, and this is beyond the scope of this paper.

[1] A. Heger, S. E. Woosley, and H. C. Spruit, Astrophys. J. **626**, 350 (2005).
[2] A. Wongwathanarat, H.-T. Janka, and E. Mueller, Astron. Astrophys. **552**, A126 (2013).
[3] C. D. Ott, E. Abdikamalov, E. O'Connor, C. Reisswig, R. Haas, P. Kalmus, S. Drasco, A. Burrows, and E. Schnetter, Phys. Rev. D **86**, 024026 (2012).
[4] C. D. Ott, E. Abdikamalov, P. Mösta, R. Haas, S. Drasco, E. P. O'Connor, C. Reisswig, C. A. Meakin, and E. Schnetter, Astrophys. J. **768**, 115 (2013).
[5] T. Kuroda, K. Kotake, and T. Takiwaki, Astrophys. J. **755**, 11 (2012).
[6] C. D. Ott, A. Burrows, T. A. Thompson, E. Livne, and R. Walder, Astrophys. J. Suppl. Ser. **164**, 130 (2006).
[7] C. A. Faucher-Giguere and V. M. Kaspi, Astrophys. J. **643**, 332 (2006).
[8] S. B. Popov and R. Turolla, Astrophys. Space Sci. **341**, 457 (2012).
[9] J. A. Pons, S. Reddy, M. Lattimer, J. M. Prakash, and J. A. Miralles, Astrophys. J. **513**, 780 (1999).
[10] J. A. Pons, J. A. Miralles, M. Prakash, and J. M. Lattimer, Astrophys. J. **553**, 382 (2001).
[11] J. A. Pons, A. W. Steiner, M. Prakash, and J. M. Lattimer, Phys. Rev. Lett. **86**, 5223 (2001).
[12] T. Fisher, S. C. Whitehouse, A. Mezzacappa, F.-K. Thielemann, and M. Liebendörfer, Astron. Astrophys. **517**, A80 (2010).
[13] N. Andersson, Classical Quantum Gravity **20**, R105 (2003).
[14] L. Franci, R. De Pietri, K. Dionysopoulou, and L. Rezzolla, Phys. Rev. D **88**, 104028 (2013).
[15] N. Andersson and K. D. Kokkotas, Int. J. Mod. Phys. D **10**, 381 (2001).
[16] H.-T. Janka, "Neutron Star Formation and Birth Properties," in *Young Neutron Stars and Their Environments*, edited by F. Camilo and B. M. Gaensler, IAU Symposium Vol. 218, (2004), http://adsabs.harvard.edu/cgi-bin/nph-data_query?bibcode=2004IAUS..218....3J&link_type=ARTICLE&db_key=AST&high=.
[17] J. M. Blondin and A. Mezzacappa, Nature (London) **445**, 58 (2007).
[18] E. Rantsiou, A. Burrows, J. Nordhaus, and A. Almgren, Astrophys. J. **732**, 57 (2011).
[19] J. O. Goussard, P. Haensel, and J. L. Zdunik, Astron. Astrophys. **321**, 822 (1997).
[20] J. O. Goussard, P. Haensel, and J. L. Zdunik, Astron. Astrophys. **330**, 1005 (1998).
[21] L. Villain, J. A. Pons, P. Cerdá-Durán, and E. Gourgoulhon, Astron. Astrophys. **418**, 283 (2004).
[22] K. Yagi and N. Yunes, Science **341**, 365 (2013).
[23] K. Yagi and N. Yunes, Phys. Rev. D **88**, 023009 (2013).
[24] A. Maselli, V. Cardoso, V. Ferrari, L. Gualtieri, and P. Pani, Phys. Rev. D **88**, 023007 (2013).
[25] D. D. Doneva, S. S. Yazadjiev, N. Stergioulas, and K. D. Kokkotas, Astrophys. J. **781**, L6 (2014).
[26] B. Haskell, R. Ciolfi, F. Pannarale, and L. Rezzolla, Mon. Not. R. Astron. Soc. Lett. **438**, L71 (2014).
[27] S. Chakrabarti, T. Delsate, N. Gürlebeck, and J. Steinhoff, Phys. Rev. Lett. **112**, 201102 (2014).
[28] J. B. Hartle, Astrophys. J. **150**, 1005 (1967).
[29] O. Benhar, V. Ferrari, L. Gualtieri, and S. Marassi, Phys. Rev. D **72**, 044028 (2005).
[30] J. B. Hartle, Astrophys. Space Sci. **24**, 385 (1973).
[31] G. B. Cook, S. L. Shapiro, and S. A. Teukolsky, Astrophys. J. **424**, 823 (1994).
[32] E. Berti and N. Stergioulas, Mon. Not. R. Astron. Soc. **350**, 1416 (2004).
[33] E. Berti, F. White, A. Maniopoulou, and M. Bruni, Mon. Not. R. Astron. Soc. **358**, 923 (2005).
[34] N. Stergioulas, RNS (1997), public domain code: http://www.gravity.phys.uwm.edu/rns.
[35] G. Pappas and T. A. Apostolatos, Phys. Rev. Lett. **108**, 231104 (2012).
[36] V. Ferrari, G. Miniutti, and J. A. Pons, Mon. Not. R. Astron. Soc. **342**, 629 (2003).
[37] V. Ferrari, G. Miniutti, and J. A. Pons, Classical Quantum Gravity **20**, S841 (2003).
[38] L. Gualtieri, J. A. Pons, and G. Miniutti, Phys. Rev. D **70**, 084009 (2004).
[39] M. Baldo, *Nuclear Methods and the Nuclear Equation of State*, International Review of Nuclear Physics Vol. 8 (World Scientific, Singapore, 1999).
[40] C. Bloch and C. De Dominicis, Nucl. Phys. **7**, 459 (1958); **10**, 509 (1959).
[41] G. F. Burgio and H.-J. Schulze, Astron. Astrophys. **518**, A17 (2010).
[42] G. F. Burgio, V. Ferrari, L. Gualtieri, and H.-J. Schulze, Phys. Rev. D **84**, 044017 (2011).
[43] D. D. Doneva, E. Gaertig, K. D. Kokkotas, and C. Krüger, Phys. Rev. D **88**, 044052 (2013).
[44] J. M. Lattimer and M. Prakash, Phys. Rep. **442**, 109 (2007).
[45] V. Dexheimer and S. Schramm, Astrophys. J. **683**, 943 (2008).
[46] S. Marassi, R. Ciolfi, R. Schneider, L. Stella, and V. Ferrari, Mon. Not. R. Astron. Soc. **411**, 2549 (2011).
[47] R. Ciolfi, V. Ferrari, and L. Gualtieri, Mon. Not. R. Astron. Soc. **406**, 2540 (2010).
[48] S. Scheidegger, R. Käppeli, S. C. Whitehouse, T. Fischer, and M. Liebendörfer, Astron. Astrophys. **514**, A51 (2010).
[49] J. Logue, C. D. Ott, I. S. Heng, P. Kalmus, and J. H. C. Scargill, Phys. Rev. D **86**, 044023 (2012).
[50] M. Bauböck, E. Berti, D. Psaltis, and F. Özel, Astrophys. J. **777**, 68 (2013).
[51] L. C. Stein, K. Yagi, and N. Yunes, Astrophys. J. **788**, 15 (2014).
[52] G. Pappas and T. A. Apostolatos, Phys. Rev. Lett. **112**, 121101 (2014).
[53] K. Yagi, K. Kyutoku, G. Pappas, N. Yunes, and T. A. Apostolatos, Phys. Rev. D **89**, 124013 (2014).
[54] T. Hinderer, Astrophys. J. **677**, 1216 (2008).
[55] K. Yagi, L. C. Stein, G. Pappas, N. Yunes, and T. A. Apostolatos, arXiv:1406.7587.
[56] J. B. Hartle and K. S. Thorne, Astrophys. J. **153**, 807 (1968).
[57] L. F. Roberts, G. Shen, V. Cirigliano, J. A. Pons, S. Reddy, and S. E. Woosley, Phys. Rev. Lett. **108**, 061103 (2012).
[58] L. F. Roberts, Astrophys. J. **755**, 126 (2012).
[59] V. R. Pandharipande, Nucl. Phys. **A174**, 641 (1971).
[60] W. D. Arnett and R. L. Bowers, Astrophys. J. Suppl. Ser. **33**, 415 (1977).

[61] R. B. Wiringa, V. Fiks, and A. Fabrocini, Phys. Rev. C **38**, 1010 (1988).
[62] J. W. Negele and D. Vautherin, Nucl. Phys. **A207**, 298 (1973).
[63] A. Akmal, V. R. Pandharipande, and D. G. Ravenhall, Phys. Rev. C **58**, 1804 (1998).
[64] R. L. Bowers, A. M. Gleeson, and R. Daryl Pedigo, Phys. Rev. C **12**, 3043 (1975).
[65] N. K. Glendenning, *Compact Stars* (Springer, New York, 2000).
[66] N. K. Glendenning, Phys. Rev. Lett. **57**, 1120 (1986).